International Journal of Applied Earth Observation and Geoinformation 20 (2013) 42–51

Contents lists available at SciVerse ScienceDirect

International Journal of Applied Earth Observation and Geoinformation

journal homepage: www.elsevier.com/locate/jag

Multiscale mapping of burn area and severity using multisensor satellite data and spatial autocorrelation analysis

A. Lanorte[a,*], M. Danese[b], R. Lasaponara[a], B. Murgante[c]

[a] CNR-IMAA, Tito Scalo, Potenza, Italy
[b] CNR-IBAM, Tito Scalo, Potenza, Italy
[c] University of Basilicata, Potenza, Italy

ARTICLE INFO

Article history:
Received 22 March 2011
Accepted 3 September 2011

Keywords:
ASTER
MODIS
Fire severity
Spatial autocorrelation statistics

ABSTRACT

Traditional methods of recording fire burned areas and fire severity involve expensive and time-consuming field surveys. Available remote sensing technologies may allow us to develop standardized burn-severity maps for evaluating fire effects and addressing post fire management activities. This paper focuses on multiscale characterization of fire severity using multisensor satellite data. To this aim, both MODIS (Moderate Resolution Imaging Spectroradiometer) and ASTER (Advanced Spaceborne Thermal Emission and Reflection Radiometer) data have been processed using geo-statistic analyses to capture pattern features of burned areas.

Even if in last decades different authors tried to integrate geo-statistics and remote sensing image processing, methods used since now are only variograms, semivariograms and kriging. In this paper, we propose an approach based on the use of spatial indicators of global and local autocorrelation. Spatial autocorrelation statistics, such as Moran's I and Getis–Ord Local Gi index, were used to measure and analyze dependency degree among spectral features of burned areas. This approach enables the characterization of pattern features of a burned area and improves the estimation of fire severity.

1. Introduction

Fire represents one of the main disturbances of Mediterranean Basin, bringing profound transformations at different temporal and spatial scales which affect ecosystems, landscapes and environments. Immediately after a fire, there are its direct effects (also known as immediate effects or first-order fire effects), which are combustion direct consequences, namely fuel consumption, production of smoke and ash and heating of soil. Whereas, since a few hours up to many decades after a fire, there are long-term results (also known as second-order fire-effects), which are indirect results of fire, namely alteration in vegetation structure and composition, soil erosion, changes in nutrient levels, micro-climate, hydrology, vegetation succession.

In the Mediterranean Basin, composition and structure of vegetation have been and are generally strongly shaped by fires, which tend to operate as a selective force, increasing species diversity, as well as a filter favouring the dominance of some species rather than of other ones (Grace et al., 2006; Pausas and Verdú, 2008).

Effects of fires on soil, plants, landscape and ecosystems depend on many factors (among them fire frequency and plant resistance). Burn severity is a qualitative indicator of the effects of fire on ecosystems, since it affects forest floor, canopy, etc. Assessing and mapping burn severity is important to monitor fire effects, to model and evaluate post-fire dynamics and to estimate the ability of vegetation to recover after fire (generally indicated as fire-resilience). In an operational context, burn severity estimation is critical for short-term mitigation and rehabilitation treatments. Traditional methods of recording fire severity involve expensive and time-consuming field surveys. The use of satellite remote sensing can help in overcoming such drawbacks.

Remote sensing technologies can provide useful data for fire management, from risk estimation (Rauste et al., 1997; Lasaponara, 2005), fuel mapping (Lasaponara and Lanorte, 2006, 2007a,b), fire detection (Lasaponara et al., 2003), to post fire monitoring (Lasaponara, 2006), including burn area and severity estimation (Gitas and Desantis, 2009; Hall et al., 2008; Richards, 1995). Methods generally used to estimate fire severity from satellite are based on spectral indexes, obtained as a combination of bands which emphasize changes induced by fire in vegetation spectral behaviour. Several vegetation indexes were used, such as SVI (Simple Vegetation Index), TVI (Transformed Difference Vegetation Index), SAVI (Soil Adjusted Vegetation Index), NDVI

* Corresponding author.
E-mail address: alanorte@imaa.cnr.it (A. Lanorte).

0303-2434/$ – see front matter © 2011 Elsevier B.V. All rights reserved.
doi:10.1016/j.jag.2011.09.005

(Normalized Difference Vegetation Index) and NBR (Normalized Burn Difference).

Maps obtained by difference between pre- and post-fire indexes provide a measure of change used to quantify biomass loss, carbon release, smoke production, etc. (Xiao et al., 2003). Such evaluations are generally performed on fire perimeter maps (a priori known), mainly using fixed threshold values to classify and map the different levels of burn severity. Nevertheless, as suggested by many authors, such fixed threshold values are generally not suitable for fragmented landscapes and inadequate for vegetation types and geographic regions different from those for which they were devised (Key and Benson, 2006; Key, 2006; Zhu et al., 2006).

In order to overcome such limitations, a new approach, based on geo-statistical analyses applied to satellite data, is herein proposed both to estimate burn area perimeter and to evaluate the different degree of burn severity. The use of robust geo-statistical analyses to process satellite data is relatively recent, even if, in last decades different authors tried to integrate geo-statistics and remote sensing image processing (Curran et al., 1998), but methods used since now are only variograms, semivariograms and kriging (some examples are Hyppänen, 1996; Atkinson and Lewis, 2000; López-Granados et al., 2005).

In this paper, we propose a more robust spatial statistics analysis approach, based on the use of spatial indicators of global and local autocorrelation to capture feature pattern, to map areas affected by fire and to estimate the degree of fire severity. For the purpose of this study, ASTER and MODIS derived indexes were processed for a significant test area located in southern Italy using Moran's I and Getis–Ord Local Gi index (see Moran, 1948; Getis and Ord, 1994).

2. Satellite data

In the present study satellite MODIS and ASTER data have been used. MODIS is a key instrument aboard Terra (EOS AM) and Aqua (EOS PM) satellites.

These data will improve our understanding of global dynamics and processes occurring on land, in oceans, and in lower atmosphere. MODIS is playing a vital role in the development of validated, global, interactive Earth system models able to predict global change accurately enough, to assist policy makers in making sound decisions concerning the protection of our environment.

Terra's orbit around the Earth is timed so that it passes from north to south across the equator in the morning, while Aqua passes south to north over the equator in the afternoon. Terra MODIS, launched on December 18, 1999 and Aqua MODIS, launched on May 4, 2002, are viewing the entire Earth's surface, acquiring data in 36 spectral bands ranging in wavelength from 0.4 μm to 14.4 μm, with a high radiometric sensitivity (12 bit).Two bands are imaged at a nominal resolution of 250 m at nadir, five bands at 500 m, and the remaining 29 bands at 1 km. A ±55-degree scanning pattern at the EOS orbit of 705 km achieves a 2330-km swath and provides global coverage every one to two days.MODIS bands used in this work are the first seven ones, corresponding to a spatial resolution of 250 and 500 m. These spectral bands are suitable for the study of vegetation characteristics. MODIS data used for this study were acquired on 14 July 2007 and 30 July 2007.

ASTER is a high resolution imaging instrument flying on Terra. It has the highest spatial resolution (15 meters VNIR) of all five sensors on Terra and collects data in the visible/near infrared (VNIR), short wave infrared (SWIR), and thermal infrared bands (TIR). Each subsystem is pointable in the crosstrack direction. The VNIR subsystem of ASTER is quite unique. One telescope of the VNIR system is nadir looking and two ones are backward looking, allowing the construction of three-dimensional digital elevation models (DEM) due to the stereo capability of different looking angles.

ASTER has a revisit period of 16 days, to any one location on the globe, with a revisit time at the equator of four days. ASTER collects approximately 8 min of data per orbit (rather than continuously). Among the 14 ASTER bands in this work we only considered the three channels in the VNIR region. For the purpose of our study, two MODIS and two ASTER multispectral images were acquired on 14 July 2007 and 30 July 2007, respectively before and after a fire occurrence (22 July 2007).

3. Classic methods: the NBR index

After a fire, the spectral behaviour of vegetation changes due to consumption of fuel, presence of ash, reduced transpiration of vegetation and increased surface temperature. All these effects increase reflectance in mid-infrared and reduce surface reflectance in near-infrared. This is the reason because NBR index (formula 1) is computed on the basis of the two burn sensitive bands, infrared (NIR) and shortwave infrared (SWIR). For this reason, it may be one of the best indexes to detect a burn area.

$$\mathrm{NBR} = \frac{\mathrm{NIR} - \mathrm{SWIR}}{\mathrm{NIR} + \mathrm{SWIR}} \quad (1)$$

Maps obtained by the difference between pre- and post-fire indexes (formula (2)) provide a measure of change which then can be used to estimate biomass loss, carbon release, aerosols production, etc. (Miller and Thode, 2007). Moreover, the difference in pre/post-burn NBR index could reflect surface change and characterize burn severity degree.

$$\mathrm{dNBR} = \mathrm{NBR}_{\mathrm{prefire}} - \mathrm{NBR}_{\mathrm{postfire}} \quad (2)$$

Some authors suggest the use of relative dNBR (formula (3)) in order to overcome the drawback linked to misclassification of low vegetated pixels that could arise using the absolute change image derived through dNBR (Miller et al., 2009). They argue that absolute change may be inappropriate to estimate ecological impacts of fire and may misclassify burn severity, especially using fixed threshold values in fragmented ecosystems with different vegetation types. Image differences could produce a misclassification in burn severity especially for low vegetated pixel characterized by small variations of pre/post-burn NBR index. The use of relative dNBR is recommended to map fire severity of historic fires, for which field data may not be available.

$$\mathrm{RdNBR} = \mathrm{dNBR}[\mathrm{abs}\ \ (\mathrm{NBR}_{\mathrm{prefire}})]^{1/2} \quad (3)$$

Moreover, the use of a relative index, here called RdNBR (3), will also enable us to make comparable burn severity estimation across space and time, that is a key issue for a landscape level analysis.

4. Spatial autocorrelation statistics

4.1. Spatial autocorrelation: basic concepts

The spatial autocorrelation concept is based on the first geography law introduced by Tobler (1970) "Everything is related to everything else, but nearest things are more related than distant things". In other terms, considering the occurrences of a spatial variable (events), spatial autocorrelation measures the degree of dependency among events, considering at the same time their similarity and their distance relationships.

In absence of spatial autocorrelation, the complete spatial randomness hypothesis is valid: the probability to have an event in one point with defined (x, y) coordinates is independent on the probability to have another event belonging to the same variable. The presence of spatial autocorrelation modifies that probability; fixed a neighbourhood for each event, it is possible to understand how much it is modified from the presence of other elements inside

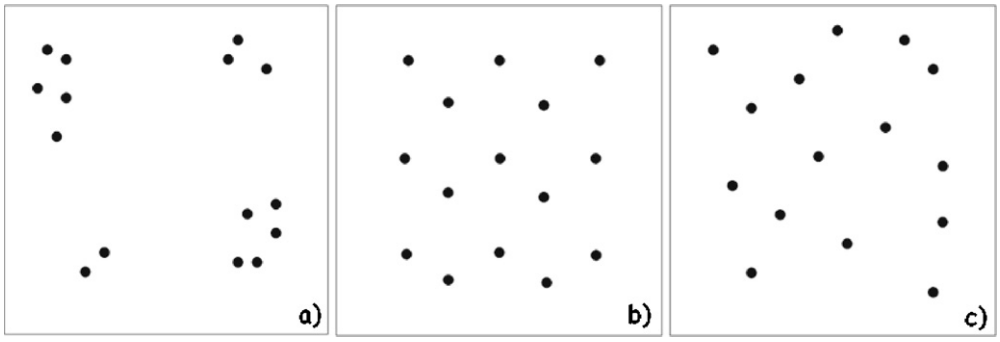

Fig. 1. Possible spatial distributions. (a) Positive spatial autocorrelation, (b) negative spatial autocorrelation and (c) null autocorrelation.

that neighbourhood.A distribution can show three types of spatial autocorrelation (O'Sullivan and Unwin, 2002):

- the variable shows positive spatial autocorrelation (Fig. 1a) when events are near and similar (clustered distribution);
- the variable shows negative spatial autocorrelation (Fig. 1b) when, even if events are near, they are not similar (uniform distribution);
- the variable shows null autocorrelation (Fig. 1c) when there are no spatial effects, neither about the position of events, or their properties (random distribution).

The presence of autocorrelation in a spatial distribution is caused by two effects, that could be clearly defined (Gatrell et al., 1996; Bailey and Gatrell, 1995), but that could not be separately studied in the practice:

- first order effects depend on properties of study region and measures how the expected value (average of the quantitative value associated to each spatial event) varies in the space with the following expression:

$$\hat{\lambda}_\tau(s) = \lim_{ds\to 0}\left\{\frac{E(Y(ds))}{ds}\right\} \tag{4}$$

where ds is neighbourhood around s, $E(\cdot)$ is the expected average and $Y(ds)$ is events number in neighbourhood;
- second order effects express local interactions between events in a fixed neighbourhood, which tend to the distance between events i and j. These effects are measured with covariance variations expressed by the limit:

$$\gamma(s_i s_j) = ds_i ds_j \overset{\lim}{\to} 0\left\{\frac{E(Y(ds_i)Y(ds_j))}{ds_i ds_j}\right\} \tag{5}$$

where symbols are similar to those used in equation 1.

As clarified by the definition of first and second order effects, the study of spatial autocorrelation requests to know in more detail:
- the quantitative nature of dataset, also called intensity of the spatial process, that is how strong a variable happens in the space (Murgante et al., 2008; Danese et al., 2009; Murgante and Danese, 2011), with the aim to understand if events are similar or dissimilar;
- the geometric nature of dataset. This needs the conceptualization of geometric relationships, usually done by the use of matrixes: (i) a distance matrix is defined to consider at which distance events influence each other (distance band); (ii) a contiguity matrix is useful to know if events influence each other; (iii) a matrix of spatial weights expresses how strong this influence is.

Concerning the distance matrix, a method should be established to calculate distances in module and direction.

For this concern Euclidean distance (3), is the most used module.

$$d_E(s_i, s_j) = \sqrt{(x_i - x_j)^2 + (y_i - y_j)^2} \tag{6}$$

For what concerns direction, existing methods take their name from the game of chess. They are called tower contiguity (Fig. 2a), bishop contiguity (Fig. 2b) and queen contiguity (Fig. 2c).

Concerning the spatial weight matrix w_{ij}, most diffused methods to calculate it are the "Inverse Distance" method and the "Fixed Distance Band" method. In the first one, weights vary in inverse relation to the distance d_{ij}^z among events:

$$w_{ij} = d_{ij}^z \tag{7}$$

where z is a number smaller then 0.

The "Fixed Distance Band" method defines a critical distance beyond which two events will never be adjacent. If the areas to which i and j belong are contiguous, w_{ij} will be equal to 1, otherwise w_{ij} will be equal to 0.

4.2. Global indicators of spatial autocorrelation

Global indicators of autocorrelation measure if and how much the dataset is autocorrelated throughout the study region.

One of the principal global indicators of autocorrelation is the Moran's index I (Moran, 1948), defined in formula (8)

$$I = \frac{N\sum_i\sum_j w_{ij}(X_i - \bar{X})(X_j - \bar{X})}{\left(\sum_i\sum_j w_{ij}\right)\sum_i (X_i - \bar{X})^2} \tag{8}$$

where N is the total pixel number, X_i and X_j are intensities in points i and j (with $i \neq j$), $\bar{X}$ is the average value, w_{ij} is an element of the weight matrix.

If $I \in [-1; 1]$; if $I \in [-1; 0]$ there is a negative autocorrelation; if $I \in [0; 1]$ there is a positive autocorrelation. Theoretically, if I converges to 0 there is null autocorrelation, in most of the cases, instead of 0 the value used to affirm the presence of null autocorrelation is given in equation (9):

$$E(I) = -\left(\frac{1}{N-1}\right) \tag{9}$$

where N is the number of events in the whole distribution.

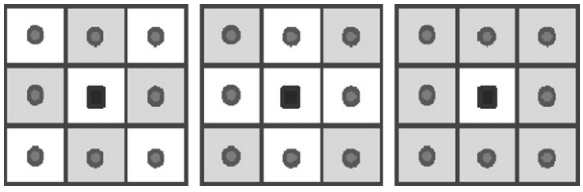

Fig. 2. (a) Tower contiguity, (b) bishop contiguity and (c) queen contiguity.

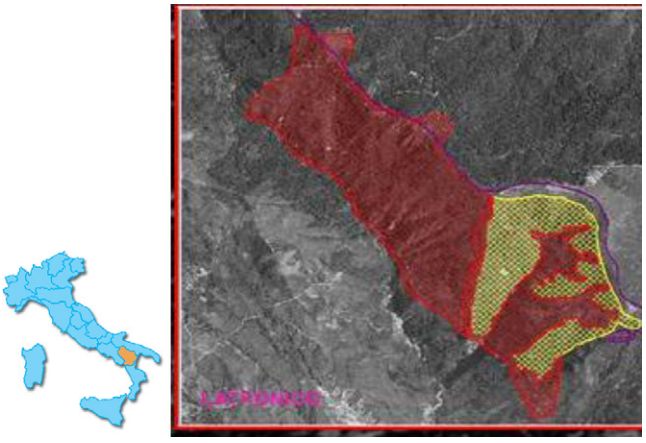

Fig. 3. Study area location: (left) orange indicates Basilicata region; (right) map of the burned area as provided by Italian Forestry Service; yellow depicts grassland and red forest cover affected by fire on 22 July 2007. (For interpretation of the references to color in this figure legend, the reader is referred to the web version of this article.)

4.3. Local indicators of spatial autocorrelation

Local indicators of spatial autocorrelation allow us to locate clustered pixels, by measuring how much features inside the fixed neighbourhood are homogeneous.

In this study we used the Getis–Ord Local Gi (Getis and Ord, 1994; Illian et al., 2008), defined according to formula (10)

$$G_i(d) = \frac{\sum_{i=1}^{n} w_i(d)x_i \; x_i \sum_{i=1}^{n} w_i(d)}{S(i)\sqrt{\left[(N-1)\sum_{i=1}^{n} w_i(d) - \left(\sum_{i=1}^{n} w_i(d)\right)^2\right] / N-2}} \qquad (10)$$

which is very similar to Moran's index, except for $w_{ij}(d)$ which, in this case, represents a weight which varies according to distance.

The interpretation of Getis and Ord's Gi meaning is not immediate, but it needs a preliminary classification that should be done comparing Gi to intensity values. In particular, a high value of the index means positive correlation for high values of intensity, while a low value of the index means positive correlation for low values of intensity.

Geostatistical analysis tools are available in several different commercial software, such as GIS and image processing ones. We used ENVI packages for the current study.

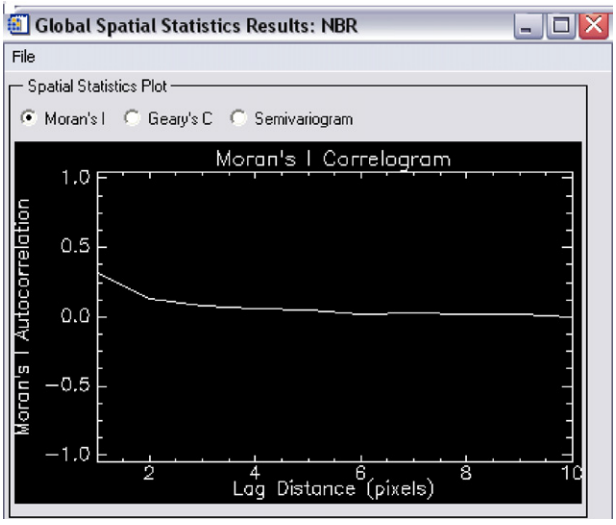

Fig. 4. Calculation of Moran's I for dNBR.

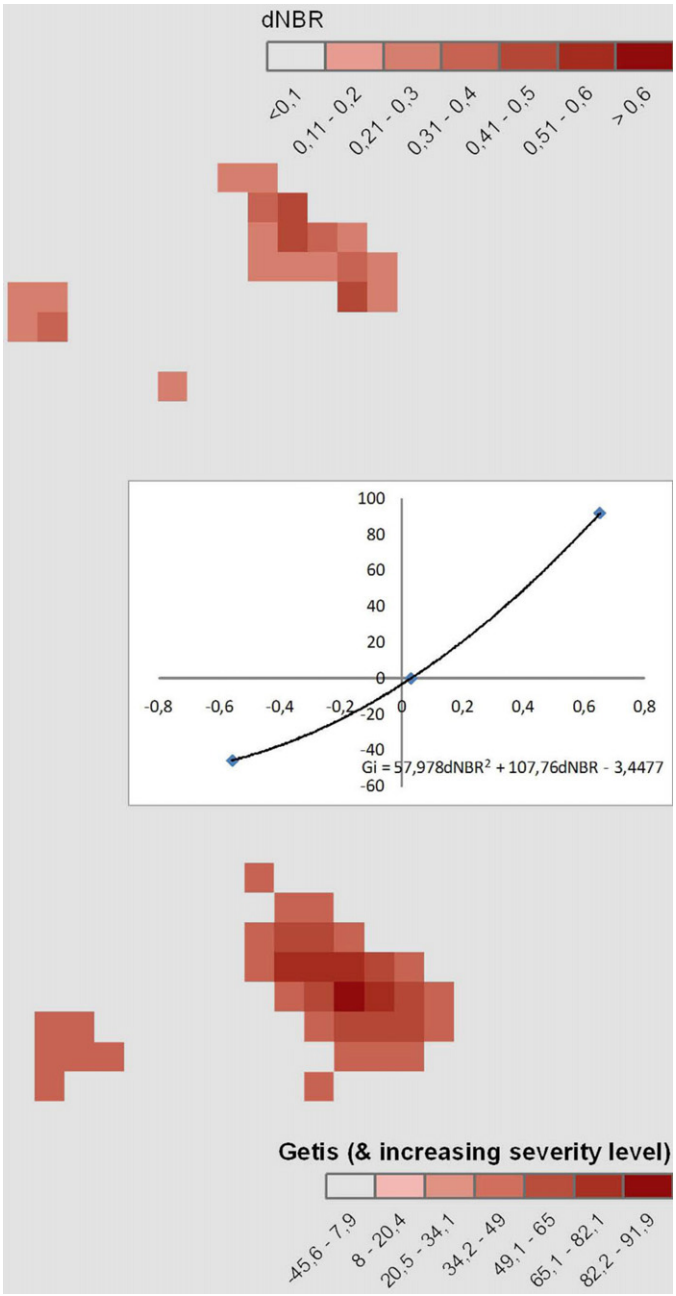

Fig. 5. Comparison between results obtained by (top) dNBR calculated for Modis datum and by (bottom) Gi calculated using dNBR as intensity. Correlation between the two indexes is shown in the white rectangle.

4.4. Spatial autocorrelation and remote sensing

In the application of spatial autocorrelation methods in remote sensing images it is important to define which are the spatial events, their quantitative nature (intensity) and the conceptualization of geometric relationships.

In the context of image processing the spatial event is the pixel and spatial autocorrelation statistics are usually calculated considering geographical coordinates of its centroid.

Concerning the intensity, it should be chosen strictly considering the empirical nature of the case of study.

The conceptualization of geometric relationships in the case of image processing is very easy, because distance between events is always equal to or is a multiple of pixel size. The contiguity

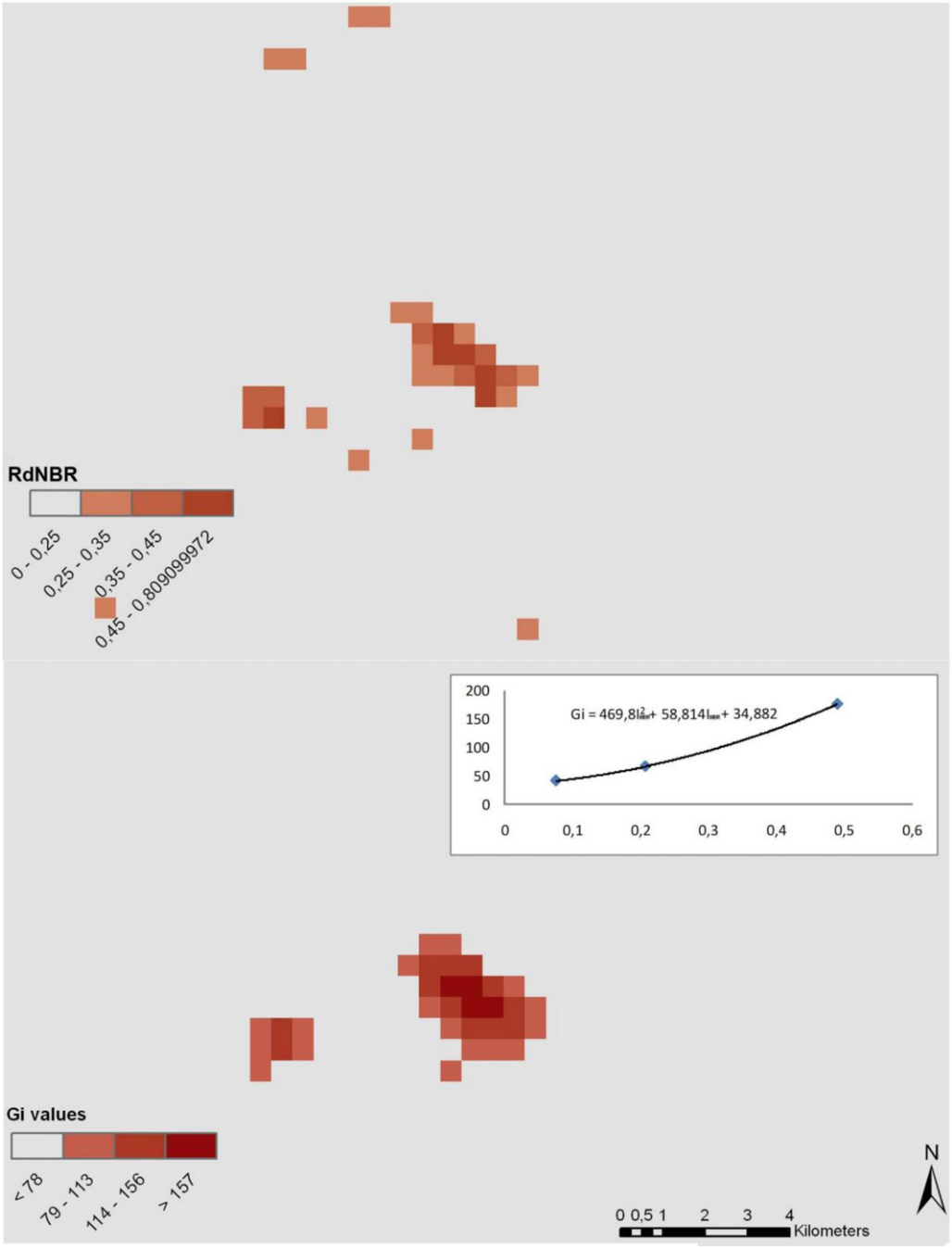

Fig. 6. Burned areas with different severity levels obtained with (top) RdNBR calculated for Modis datum and with (bottom) Gi calculated using RdNBR as intensity. Correlation between the two indexes is shown in the white rectangle.

distance is called in the image processing lag distance. The application of spatial autocorrelation statistics in remote sensed image allows us to obtain a new raster which contains in each pixel a number that expresses how much it is autocorrelated with other pixels.

5. Data processing and results

5.1. Study area and data set

The study was carried out in Basilicata Region (South of Italy), which in the last years has been characterized by an increasing number of fires, generally occurring during the dry season from July to September. Spatial statistical analyses were carried out for a significant fire event occurred in the municipality of Latronico (Pz), with an extension of 261 ha. The area is characterized by grasslands, Mediterranean maquis, broadleaf forest and transitional woodland–shrub cover. Fig. 3 shows the location of study area along with the map of burned area carried out by Italian Forestry Service. Yellow areas are related to burned grassland and red areas are related to forest cover affected by fire.

Both MODIS and ASTER data were used to compute dNBR map and further processed to assess burned areas and fire severity using geostatistical analyses described in Section 4.

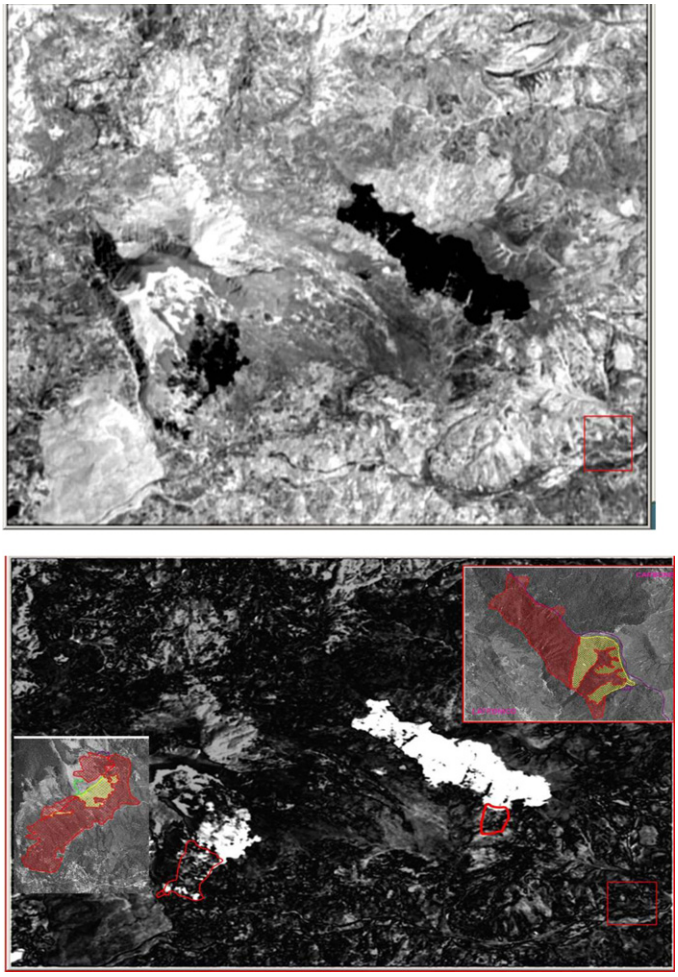

Fig. 7. Fire scars as obtained from satellite images (top), Latronico Fires Maps of burned areas from field surveys made by fire brigate (Corpo Forestale dello Stato) (bottom).

5.2. MODIS data processing and results

First, MODIS data were used to compute the following indexes, by using MODIS spectral bands 2 (841–876 nm) and 7 (2105–2155 nm) with a spatial resolution of 500 m.

$$\mathrm{NBR}_{\mathrm{MODIS}} = \frac{\mathrm{MODIS}_2 - \mathrm{MODIS}_7}{\mathrm{MODIS}_2 + \mathrm{MODIS}_7} \quad (11)$$

Using these two bands we obtained a NBR map which is particularly sensitive to changes occurring in vegetation cover affected by fire, such as amount of live green vegetation, moisture content, etc. NBR values generally range between 1 and −1 as well as NDVI. Strongly negative NBR values would indicate a larger reflectance in SWIR than NIR band, and this only occurs over not vegetated areas where fire cannot occur.

In order to well characterize and identify burned areas, we computed and used delta NBR (dNBR) expected to perform better than other methods in capturing the spatial complexity of severity within fire perimeters. Positive dNBR values represent a decrease in vegetation while negative values represent increased vegetation cover. Finally another index was calculated, here called I_{MODIS} (12), obtained from the NBR computed pre- and post-fire occurrence.

$$\mathrm{RdNBR}_{\mathrm{MODIS}} = \frac{\mathrm{NBR}_{\mathrm{prefire}} - \mathrm{NBR}_{\mathrm{postfire}}}{\sqrt{|\mathrm{NBR}_{\mathrm{prefire}}|}} \quad (12)$$

Table 1
Severity categories: dNBR and RdNBR thresholds from (Miller and Thode, 2007).

Severity category	dNBR	RdNBR
Unchanged	<41	<69
Low	41/176	69/315
Moderate	176/366	316/640
High	>366	>640

The intensity is generally chosen, considering the main feature of phenomenon to analyze. In this paper, we used two types of intensity, computed using Eqs. (11) and (12), respectively.

In other words, Moran's I and Getis and Ord's Gi were calculated using first $\mathrm{dNBR}_{\mathrm{MODIS}}$ (expressed by Eq. (11)) and then $\mathrm{RdNBR}_{\mathrm{MODIS}}$ (expressed by Eq. (12)) as intensity.

For all these cases, the first step was the use of the global indicator to obtain lag distance useful to calculate Gi, which was performed using queen's contiguity, selected in order to conduct the analysis in all directions.

To find the optimal lag distance, global Moran's I was used and calculated for different values of lag distances. The best value is the lag that maximizes I (Fig. 4) and captures image autocorrelation in the best way. The lag found in both cases is 2 pixels.

At this point, local indicators of spatial association were calculated using lag distance found and queen's contiguity.

Results from this assessment are shown in Figs. 5 and 6 where burned areas are obtained with (see figures bottom) and without (see figures top) the use of geo-statistical analysis.

In particular, Fig. 5 shows the comparison between different MODIS classification results obtained from (top) $\mathrm{dNBR}_{\mathrm{MODIS}}$ and (bottom) Gi calculated using the $\mathrm{dNBR}_{\mathrm{MODIS}}$ as intensity. Intensities ($\mathrm{dNBR}_{\mathrm{MODIS}}$ and $\mathrm{RdNBR}_{\mathrm{MODIS}}$) and their respective Gi were classified according to the following steps:

- $\mathrm{dNBR}_{\mathrm{MODIS}}$ was classified finding empirically its minimum and maximum value in the burned area. Range between such values was then split in equal classes;
- I_{NBR} was classified with the same method applied to $\mathrm{dNBR}_{\mathrm{MODIS}}$ raster;
- Gi was classified considering a parabolic relationship found between Gi values and intensity used for its calculation each time. So Figs. 5 and 8 contain parabolic relationships found between $\mathrm{dNBR}_{\mathrm{MODIS}}$ and Gi while Figs. 6 and 9 contain parabolic relationships found between $\mathrm{RdNBR}_{\mathrm{MODIS}}$ and Gi.

Considering point (i) it should be noticed that we obtained seven classes ranging from 0.1dNBR to 0.6dNBR. In order to assess the physical significance of analyses, we compared our classes and range values to results obtained by independent studies (Miller and Thode, 2007) conducted in different geographical areas using field observations. We found a strong consistency between our range values and those indicated by Miller and Thode (2007), except for the fact that the authors scaled $\mathrm{NBR}_{\mathrm{MODIS}}$ by 1000 to transform data to integer format. Therefore, if we rescale dNBR values to be compared, the seven classes we obtained are now ranging from 100 $\mathrm{dNBR}_{\mathrm{MODIS}}$ to 600 $\mathrm{dNBR}_{\mathrm{MODIS}}$, which means that all classes we obtained are related to burned area from low to high values. Considering point (ii), it should be noticed that we obtained 4 classes and making the same considerations for $\mathrm{RdNBR}_{\mathrm{MODIS}}$ as previously done for dNBR we obtained that the last three classes ranging from 250 to 800 are related to burned areas from low to high values of fire severity category, identified by Miller and Thode (2007) using field survey and listed in Table 1.

Considering that the classification is carried out using both Gi and intensity values, it should be noted that: (i) a high value of Getis and Ord's Gi means positive correlation for high values of intensity,

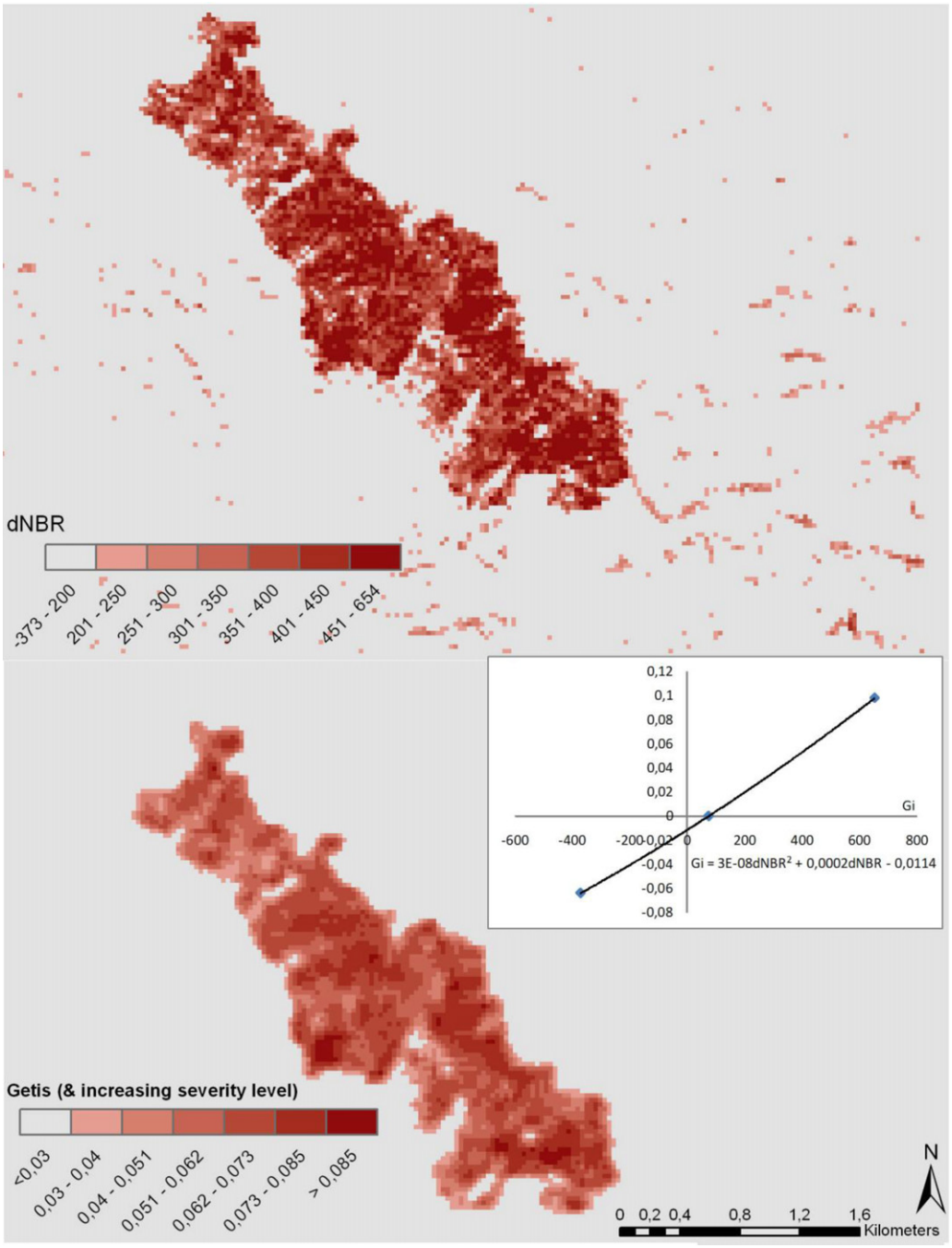

Fig. 8. Burned areas with different severity levels obtained with (top) dNBR calculated for Aster datum and with (bottom) Gi calculated using dNBR as intensity. Correlation between the two indexes is shown in the white rectangle.

thus providing pixels strongly affected by fire and characterized by high fire severity level, (ii) while a low value of Getis and Ord's Gi index means positive correlation for low values of intensity, thus providing pixels characterized by low levels of fire severity or unaffected by fire. The correlation between the two indexes is shown in the white rectangle in Fig. 5.

From a visual inspection of Fig. 5, we can notice that results obtained by (top) $dNBR_{MODIS}$ exhibit some pixels which could not have been affected by fire. A similar behaviour can be observed in the results of (bottom) Gi calculated using dNBR as intensity.

In Fig. 5 (top and bottom), some problems appear to be present: (i) the overestimation of burned area, and (ii) the presence of additional pixels classified as burned area. The overestimation of burned area is due to pixel size which is not adequate for detecting a fire-affected area of about 200 ha. Of course, the whole pixel is classified as burned even if only a small part of it is affected by fire.

To check reliability of obtained results, we also considered intensity obtained by means of Eq. (10), which should be able to better classify fire affected pixels. Such results are shown in Fig. 6 where burned areas are obtained with (see bottom) and without (see top) the use of geo-statistical analysis. Areas with different fire severity levels were obtained with (top) RdNBR calculated for MODIS images and with (bottom) Gi calculated using RdNBR as intensity. Correlation between the two indexes is shown in the white rectangle.

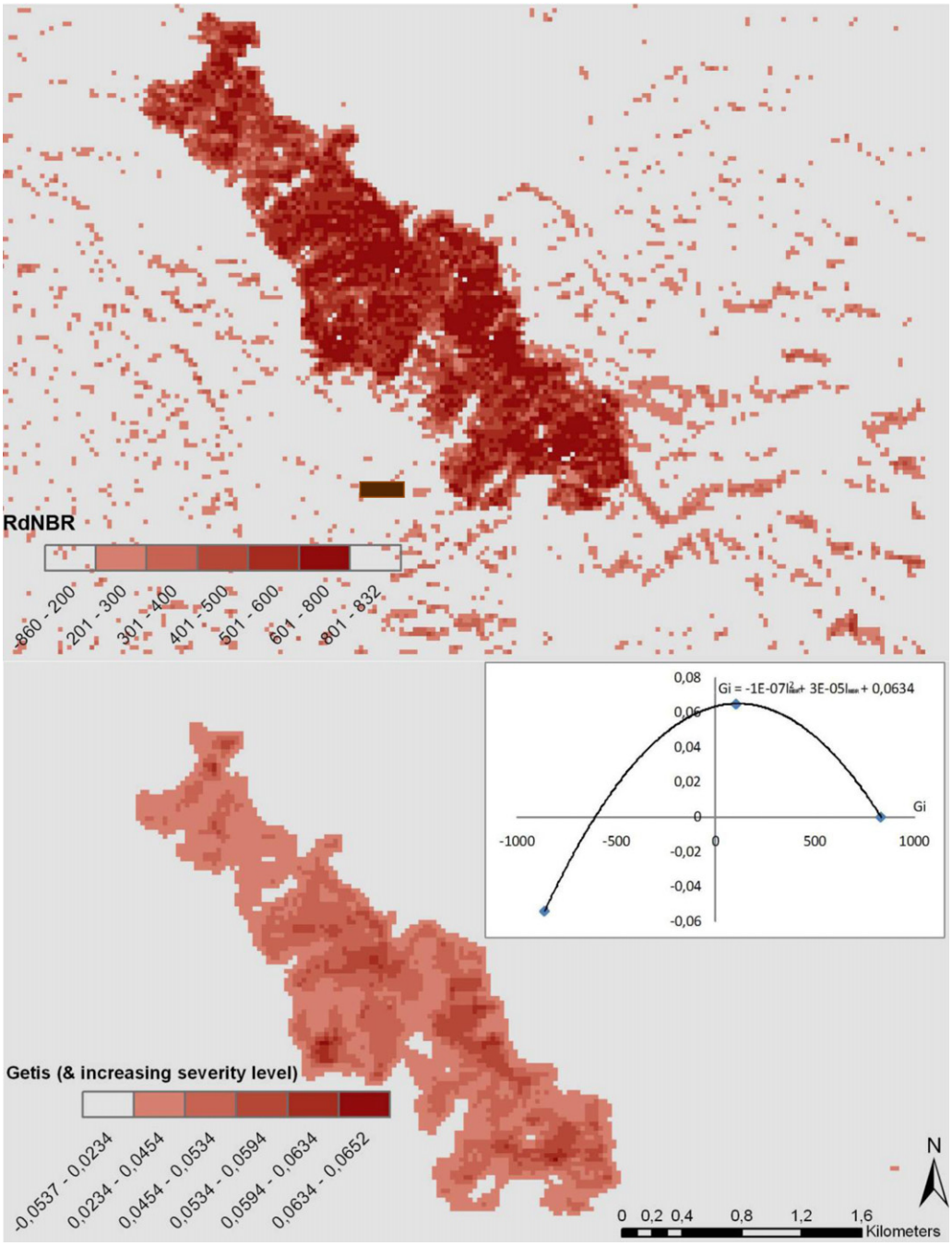

Fig. 9. Burned areas with different severity levels obtained with (top) RdNBR calculated for Aster datum and with (bottom) Gi calculated using RdNBR as intensity. Correlation between the two indexes is shown in the white rectangle.

Fig. 6 (bottom) clearly shows that the classification carried out using both Gi and intensity values enabled us to exclude sporadic pixels wrongly classified as fire affected using only RdNBR index, whereas a group of seven pixels (Fig. 6, bottom) is still present. A comparison with field surveys clearly suggests that this area is correctly classified as burned area linked to an additional fire of about 200 ha occurred in the same period (26 July 2007) very close to the fire of our concern as highlighted in Fig. 7.

Of course, the overestimation of the burned area is still due to pixel size, but the joint use of spectral indexes and statistical analyses enables us to correctly classify the burned area and to discriminate fire severity.

The use of spatial statistics allows us to obtain improved identification of burned areas and, consequently, of fire severity classifications for both the investigated indexes dNBR and RdNBR.

5.3. ASTER data processing and results

To evaluate the results obtained from MODIS data for the fire under investigation, we also elaborated ASTER satellite images. As in the previous case for MODIS, also ASTER data were used to assess burned areas and fire severity with and without the use of geostatistical analyses described in Section 4.

ASTER data were used to compute NBR based indexes using ASTER 3 (760–860 nm) and 7 (2235–2285 nm) spectral channels, with a spatial resolution of 30 m, using formula (13).

$$NBR_{ASTER} = \frac{ASTER_2 - ASTER_7}{ASTER_2 + ASTER_7} \quad (13)$$

In this case NBR_{ASTER} values were multiplied by 1000 and converted to integer format to follow Miller and Thode (2007) and compare NBR_{ASTER}. As in the previous case for MODIS, another index was calculated, here called $RdNBR_{ASTER}$ (see formula (14)), obtained from NBR computed pre- and post-fire occurrence.

$$RdNBR_{ASTER} = \frac{NBR_{prefire} - NBR_{postfire}}{\sqrt{|NBR_{prefire}/1000|}} \quad (14)$$

Since we scaled NBR by 1000 to transform data to integer format, in formula 14 the pre-fire NBR must be divided by 1000. Taking the absolute value of pre-fire, NBR in the denominator allows computing the square-root without changing the sign of original dNBR.

Fig. 8 depicts Aster burned areas with different severity levels obtained by $dNBR_{aster}$ (top) and Gi (bottom) calculated using $dNBR_{aster}$ as intensity. Correlation between the two indexes is shown in the white rectangle. Results were found with the same classification method used for MODIS images. Again, a parabolic relationship was found between intensity and Getis and Ord's Gi. Applying this relationship, significant values of Gi were found corresponding to $dNBR_{aster}$ classes.

As previously done for MODIS data investigations, considering point (i) of Section 5.2 we obtained several fire severity classes, whose range values were compared with results obtained from Miller and Thode (2007). We found a strong consistency between our classes and range values indicated by Miller and Thode (2007) on the basis of field surveys. In particular, the last five classes we obtained were higher than 200 and therefore they correspond to moderate and high fire severity according to severity category by Miller and Thode (2007) herein listed in Table 1. Nevertheless, when we applied this classification to the whole ASTER $dNBR_{aster}$ image, a high number of pixels were identified as burned area with fire severity levels ranging from moderate to high. As it is shown in Fig. 8 (bottom), also in the case of ASTER $dNBR_{aster}$ images, the application of spatial statistics enabled us to improve both the detection of burned areas and the assessment of fire severity levels. The classification of Gi (bottom), calculated using dNBR as intensity, excluded unburned areas.

Finally, Fig. 9 shows different severity levels obtained by $RdNBR_{ASTER}$ (top) and Gi (bottom) calculated using $RdNBR_{ASTER}$ as intensity. Correlation between the two indexes is shown in the white rectangle.

The visual comparison between bottom and top of Fig. 9 clearly shows that the classification carried out using both Gi and intensity values enabled us to exclude sporadic pixels wrongly classified as burned areas using only RdNBR index. A comparison with field surveys clearly suggests that (i) this area is correctly classified as burned area and (ii) fire severity categories well identified the different levels of fire severity.

In particular, both mapping of the entire burned area and corresponding to different levels of fire severity, have been reached with GPS tracking.

Results from all performed analyses pointed out that, for both MODIS and ASTER images, a parabolic relationship was found between intensity and Getis and Ord's Gi. Applying this relationship, significant values of Gi were found corresponding to dNBR classes. Obtained results enable us to recognize fire burned areas and quantitatively characterize fire patterns and burn severity.

Of course, the use of Aster images limited the overestimation of burned areas due to a most adequate pixel size for investigated small fires (around 200 ha). Finally, the joint use of spectral indexes and statistical analyses enables us to correctly detect burned areas and to assess fire severity using both investigated indices dNBR and RdNBR.

6. Conclusions

In this paper, we propose a robust statistical approach, based on the use of spatial indicators of global and local autocorrelation, to detect burned area and estimate fire severity. Spatial autocorrelation statistics, such as Moran's I and Getis–Ord Local Gi index (see Moran, 1948; Getis and Ord, 1994), were used to capture pattern features of burned areas.

We focused on the multiscale analyses using both MODIS (Moderate Resolution Imaging Spectroradiometer) and ASTER (Advanced Spaceborne Thermal Emission and Reflection Radiometer) data to identify burned areas and characterize burn severity. Pre- and post-fire satellite MODIS and ASTER images were processed for a significant test area in Southern Italy. Spectral indexes generally used for fire severity estimation were analyzed and processed with and without using geostatistical analyses.

The comparison of results obtained for both MODIS and ASTER images with and without the use of spatial autocorrelation statistics clearly pointed out the improvements achieved using both global and local spatial autocorrelation statistics. Our results showed that these statistics applied to MODIS and ASTER data allowed us (i) to detect burned areas and (ii) to discriminate fire severity.

The new approach is independent on sensors used for the evaluation as well as on vegetation cover types affected by fire, being the value obtained really close to those obtained by independent studies carried out in diverse geographic regions and land cover types.

Assessing and mapping burn severity is important for monitoring fire effects, modeling and evaluating post-fire dynamics and estimating vegetation resilience, which is the ability of vegetation to recover after fire. The availability of satellite high resolution imagery provides the opportunity to obtain useful information for fire management, from risk evaluation to post-fire damage estimation.

The herein proposed approach could be directly incorporated into mapping process from local up to global scale.

References

Atkinson, P.M., Lewis, P., 2000. Geostatistical classification for remote sensing: an introduction. Computers & Geosciences 26, 362–371.
Curran, P., Atkinson, P.M., 1998. Geostatistics remote sensing. Progress in Physical Geography 22 (1), 61-78.
Bailey, T.C., Gatrell, A.C., 1995. Interactive Spatial Data Analysis. Longman Higher Education, Harlow.
Danese, M., Lazzari, M., Murgante, B., 2009. Geostatistics in historical macroseismic data analysis. Transactions on Computational Sciences Journal VI LNCS vol. 5730, 324–341, doi:10.1007/978-3-642-10649-1_19.
Gatrell, A.C., Bailey, T.C., Diggle, P.J., Rowlingson, B.S., 1996. Spatial point pattern analysis and its application in geographical epidemiology. Transaction of Institute of British Geographer 21, 256–271.
Getis, A., Ord, J.K., 1994. The analysis of spatial association by use of distance statistics. Geographical Analysis 24, 189–206.
Gitas, I., Desantis, A., 2009. Remote sensing of burn severity. In: Chuvieco, E. (Ed.), Earth Observation of Wildland Fires in Mediterranean Ecosystems, vol. 129. Springer-Verlag, Berlin/Heidelberg, doi:10.1007/978-3-642-01754-4_10.
Grace, J.B., Keeley, J.E., 2006. A structural equation model analysis of postfire plant diversity in California shrublands. Ecological Applications 16, 503–514.
Hall, R.J., Freeburn, J.T., de Groot, W.J., Pritchard, J.M., Lynham, T.J., Landry, R., 2008. Remote sensing of burn severity: experience from western Canada boreal fires. International Journal of Wildland Fire 17 (4), 476–489, doi:10.1071/WF08013.
Hyppänen, H., 1996. Spatial autocorrelation and optimal spatial resolution of optical remote sensing data in boreal forest environment. International Journal of Remote Sensing 17 (17), 3441–3452.
Illian, J., Penttinen, A., Stoyan, H., Stoyan, D., 2008. Statistical Analysis and Modelling of Spatial Point Patterns. Wiley.
Key, C.H., 2006. Ecological and sampling constraints on defining landscape fire severity. Fire Ecology 2 (2), pp. 178–203.

Key, C.H., Benson, N.C., 2006. Landscape assessment: Ground measure of severity, the Composite Burn Index, and remote sensing of severity, the Normalized Burn Ratio, in: Lutes, DC, Keane, R.E., Caratti, J.F., Key, C.H., Benson, N.C., Sutherland, S., Gangi, L.J. (Eds.) FIREMON: Fire Effects Monitoring and Inventory System. USDA Forest Service, Rocky Mountain Research Station, Ogden, UT. Gen. Tech. Rep. RMRS-GTR-164-CD: LA 1–51, 2006.

Lasaponara, R., 2005. Inter-comparison of AVHRR-based fire danger estimation methods. International Journal of Remote Sensing vol. 26 (5), 853–870.

Lasaponara, A., Lanorte:, 1., 2007a. VHR QuickBird data for fuel type characterization in fragmented landscape. Ecological Modelling vol. 204, 79–84.

Lasaponara, R., Lanorte:, A., 2007b. Remotely sensed characterization of forest fuel types by using satellite ASTER data. International Journal of Applied Earth Observations and Geoinformation vol. 9, 225–234.

Lasaponara, R., Lanorte, A., 2006. Multispectral fuel type characterization based on remote sensing data and Prometheus model. Forest Ecology and Management vol. 234, S226.

Lasaponara, R., Cuomo, V., Macchiato, M.F., Simoniello, T., 2003. A self-adaptive algorithm based on AVHRR multitemporal data analysis for small active fire detection. International Journal of Remote Sensing 24 (8), 1723–1749.

Lasaponara, R., 2006. Estimating spectral separability of satellite derived parameters for burned areas mapping in the Calabria Region by using SPOT-Vegetation data. Ecological Modelling vol. 196, 265–270.

López-Granados, F., Jurado-Expósito, M., Peña-Barragán, J.M., García-Torres, L., 2005. Using geostatistical and remote sensing approaches for mapping soil properties. European Journal of Agronomy 23, 279–289.

Miller, J.D., Thode, A.E., 2007. Quantifying burn severity in a heterogeneous landscape with a relative version of the delta Normalized Burn Ratio (dNBR). Remote Sensing of Environment 109, 66–80.

Miller, J.D., Knapp, E.E., Key, C.H., Skinner, C.N., Isbell, C.J., Creasy, R.M., Sherlock, J.W., 2009. Calibration and validation of the relative differenced Normalized Burn Ratio (RdNBR) to three measures of fire severity in the Sierra Nevada and Klamath Mountains, CA, USA. Remote Sensing of Environment 113 (3), 645–656.

Moran, P., 1948. The interpretation of statistical maps. Journal of the Royal Statistical Society 10, 243–251.

Murgante, B., Las Casas, G., Danese, M., 2008. The periurban city: geo-statistical methods for its definition. In: Coors, M., Rumor, V., Fendal, E.M., Zlatanova, ST. (Eds.), Urban and Regional Data Management. Taylor & Francis Group, London, pp. 473–485.

Murgante, B., Danese, M., 2011. Urban versus Rural: the decrease of agricultural areas and the development of urban zones analyzed with spatial statistics. International Journal of Agricultural and Environmental Information Systems 2 (2), 16–28, doi:10.4018/jaeis.2011070102.

O'Sullivan, D., Unwin, D., 2002. Geographic Information Analysis. John Wiley & Sons.

Pausas, J.G., Verdú, M., 2008. Fire reduces morphospace occupation in plant communities. Ecology 89 (8), 2181–2186.

Rauste, Y., Herland, E., Frelander, H., Soine, K., Kuoremaki, T., Ruokari, A., 1997. Satellite-based forest fire detection for fire control in boreal forests. International Journal of Remote Sensing 18, 2641–2656.

Richards, G., 1995. A general mathematical framework for modeling twodimensional wildland fire spread. International Journal of Wildland Fire 5 (2), 63–72.

Tobler, W.R., 1970. A computer model simulating urban growth in the detroit region. Economic Geography 46, 234–240.

Xiao, X., Braswell, B., Zhang, Q., Boles, S., Frolking, S., Moore III, B., 2003. Sensitivity of vegetation indices to atmospheric aerosols: continental-scale observations in Northern Asia. Remote Sensing Environment 84, 385–392.

Zhu, Z., Key, C., Ohlen, D., Benson, N., 2006. Evaluate sensitivities of burn-severity mapping algorithms for different ecosystems and fire histories in the United States. Final Report to the Joint Fire Science Program, Project JFSP 01-1-4-12, October 12, 35 pp., 2006.